AD_____

Award Number: DAMD17-01-1-0125

TITLE: The Role of Actin Polymerization in Tumor Metastasis

PRINCIPAL INVESTIGATOR: Xi Zhan, Ph.D.

CONTRACTING ORGANIZATION: American Red Cross
Rockville, Maryland 20855

REPORT DATE: August 2004

TYPE OF REPORT: Final

PREPARED FOR: U.S. Army Medical Research and Materiel Command
Fort Detrick, Maryland 21702-5012

DISTRIBUTION STATEMENT: Approved for Public Release;
Distribution Unlimited

The views, opinions and/or findings contained in this report are
those of the author(s) and should not be construed as an official
Department of the Army position, policy or decision unless so
designated by other documentation.

20050407 122

REPORT DOCUMENTATION PAGE

Form Approved
OMB No. 074-0188

Public reporting burden for this collection of information is estimated to average 1 hour per response, including the time for reviewing instructions, searching existing data sources, gathering and maintaining the data needed, and completing and reviewing this collection of information. Send comments regarding this burden estimate or any other aspect of this collection of information, including suggestions for reducing this burden to Washington Headquarters Services, Directorate for Information Operations and Reports, 1215 Jefferson Davis Highway, Suite 1204, Arlington, VA 22202-4302, and to the Office of Management and Budget, Paperwork Reduction Project (0704-0188), Washington, DC 20503

1. AGENCY USE ONLY (Leave blank)	2. REPORT DATE August 2004	3. REPORT TYPE AND DATES COVERED Final (1 Aug 2001 - 31 Jul 2004)

4. TITLE AND SUBTITLE
The Role of Actin Polymerization in Tumor Metastasis

5. FUNDING NUMBERS
DAMD17-01-1-0125

6. AUTHOR(S)
Xi Zhan, Ph.D.

7. PERFORMING ORGANIZATION NAME(S) AND ADDRESS(ES)
American Red Cross
Rockville, Maryland 20855

E-Mail: zhanx@usa.redcross.org

8. PERFORMING ORGANIZATION REPORT NUMBER

9. SPONSORING / MONITORING AGENCY NAME(S) AND ADDRESS(ES)
U.S. Army Medical Research and Materiel Command
Fort Detrick, Maryland 21702-5012

10. SPONSORING / MONITORING AGENCY REPORT NUMBER

11. SUPPLEMENTARY NOTES

12a. DISTRIBUTION / AVAILABILITY STATEMENT
Approved for Public Release; Distribution Unlimited

12b. DISTRIBUTION CODE

13. ABSTRACT (Maximum 200 Words)

Breast cancer is frequently associated with gene amplification of EMS1 or cortactin, a protein that regulates the assembly of filamentous actin (F-actin). Previous studies have demonstrated that overexpression of cortactin results in increase in metastases and invasion of breast tumor cells. The goal of this project is to reveal the potential to target cortactin in tumor metastasis with initial emphasis on the biological significance of the interaction of cortactin with phospholipids, which are known to play a critical role in the modulation of cell migration in response to extracellular stimuli and other cellular proteins. Cortactin binds to a subset of phosphatidylinositides, including phosphatidylinositol 5-phosphoate (PI(5)P), phosphatidylinoistol 4,5 biophosphoate (PI(4,5)P2) and phosphatidylinositol 4-phosphoate (PI(4)P). Interestingly, not all those phospholipids show a similar effect on the activity of cortactin. While PI(5)P increases the activity of cortactin for actin assembly, PI(4)P inhibits the cortactin mediated actin branching. This data indicates that the activity of cortactin is regulated by different types of membrane phospholipids. Our recent study has also identified that cortactin binds to missing in metastasis (MIM), which is frequently under expressed in many malignant cells. Binding of MIM to cortactin appears to be regulated by extracellular stimuli such as PDGF and requires tyrosine phosphorylation of cortactin. Furthermore, interaction with MIM potentiates the activity of cortactin but inhibits N-WASP for actin polymerization. More significantly, overexpression of MIM inhibits tumor cell motility. These data indicate that interaction between cortactin and MIM may play an important role in tumor metastasis.

14. SUBJECT TERMS
Breast Cancer

15. NUMBER OF PAGES
60

16. PRICE CODE

17. SECURITY CLASSIFICATION OF REPORT Unclassified	18. SECURITY CLASSIFICATION OF THIS PAGE Unclassified	19. SECURITY CLASSIFICATION OF ABSTRACT Unclassified	20. LIMITATION OF ABSTRACT Unlimited

NSN 7540-01-280-5500

Standard Form 298 (Rev. 2-89)
Prescribed by ANSI Std. Z39-18
298-102

Table of Contents

Introduction

Breast cancer is frequently associated with gene amplification of the chromosome 11q13, resulting in overexpression of cortactin, a cortical actin-associated protein and a prominent substrate of protein tyrosine kinase Src. Cortactin is accumulated in peripheral structures of cells including lamellipodia and membrane ruffles where cortical actin is enriched. In MDA-MB-231 breast cancer cells plated on extracellular matrix cortactin is enriched in invadopodia, a type of membrane protrusions that participates in degradation of and invasion into the matrix. While the precise role of cortactin in tumor progression remains unclear, amplification and overexpression of cortactin appear to be intimately associated with patients with poor prognosis or relapse, indicating that overexpression of cortactin may contribute to a late stage of tumor progression. This notion is further strengthened by our recent study showing that MDA-MB-231 cells overexpressing wild-type cortactin acquired higher potential for cell migration in vitro and tumor invasion and metastasis in vivo. The protein sequence of cortactin is featured by six and one half tandem copies of a unique 37-amino-acid repeat and a Src homology 3 (SH3) domain at the carboxyl terminus. Our recent study also demonstrated that cortactin binds via its N-terminus to Arp2/3 complex, a primary machinery for actin polymerization. Such interaction plays a critical role in the regulation of actin cytoskeleton in cell leading edges. Studies from this laboratory have further found that cortactin interacts with a certain type of phosphatidylinositides, which bind to the plasma membrane and are known to be implicated in the regulation of the cytoskeleton. Therefore, we hypothesize that the association of cortactin with these phospholipids may be important for the dynamics of actin cytoskeleton at the cell leading edge and play a role in tumor invasion and metastasis. The project funded by this grant is to characterize the detail of the interaction of cortactin with phospholipids and seek for opportunities by which we may be able to compromise metastasis.

Body

Task: Study the effects of phosphatidylinositides on the activity of cortactin-mediated actin polymerization and structural elements essential for the association of cortactin with phospholipids

The rationale to study cortactin phosphatidylinositide association is to investigate the regulation of the activity of cortactin. While our study in the previous year demonstrated that cortactin binds to multiple types of phospholipids, PI(4)P and PI(5) appeared to be the strongest affinity for cortactin. To define the significance of the binding of these types of lipids on the function of cortactin, we examined the effect of PI(4)P and PI(5)P on the function of cortactin. Synthetic PI(5)P, PI(4,5)P_2, PI(4)P (Echelon Biosciences) were suspended in chloroform and transferred to glass vessels. The chloroform was removed by vacuum. The lipid film was resuspended in buffer (10 mM imidazole [pH 7.0], 50 mM KCl, 1 mM EGTA, 1 mM MgCl$_2$) by vortexing in a 37°C water-bath, and subjected to sonication for 10 min. The resulting liposome was added in actin polymerization reaction containing 1.5 µM Mg-ATP G-actin, Arp2/3 complex and cortactin at concentrations as indicated. Pyrene fluorescence was measured at excitation at 365 nm and emission at 407 nm, and the value was collected on a LS50B spectrofluorometer (Perkin Elmer) at a rate of 1 point every 3s. As shown in Figure 1A, the activity of cortactin in the stimulation of Arp2/3 complex for actin polymerization is significantly enhanced by PI(5)P, not by PI(4,5)P_2. Interestingly, PI(4)P inhibits significantly cortactin/Arp2/3 mediated actin assembly at concentration of 100 µM (Figure 1B). The effect of phospholipids on actin branching was also examined (Figure 2). While the actin assembled in the presence of Arp2/3 complex/cortactin or in addition to PI(5)P were significantly branched, those in the presence of PI(4)P were long with little branching. This result indicates specificities of PI(4)P and PI(5)P on cortactin.

In addition, we have established a series of small interference RNA (siRNA) to inhibit the expression of cortactin in MDA-MB-231 cells. Two of these RNAs can effectively knock down cortactin by more than 80%. In a collaboration with Susette Muller in Georgetown, we have found that cortactin siRNA can inhibit invadopodia formation of tumor cells.
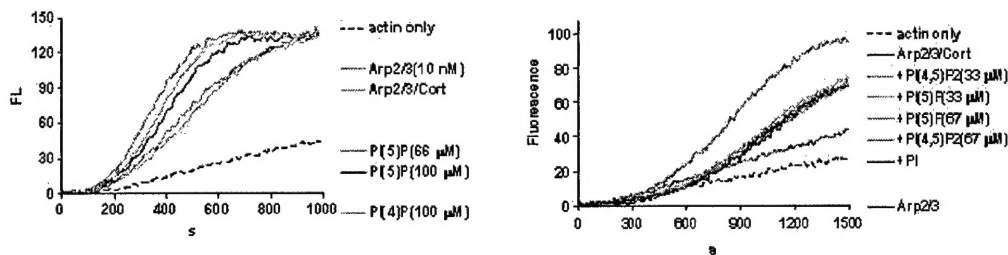
Figure 1. The effect of phosphatidylinositol 5-phosphate (PI(5)P, phosphosphatidylinositol 4-phosphoate (PI(4)P and phosphatidylinositol 4,5-biophosphates (PI(4,5)P2 on cortactin/Arp2/3 mediate actin assembly
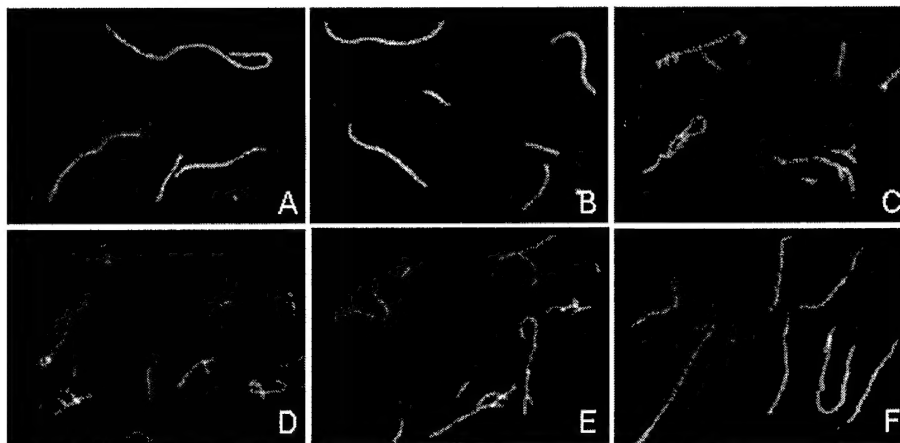

Figure 2. Effect of PIPs on actin branching induced by Arp2/3 complex and cortactin. (A) Actin only, (B) Arp2/3 only, (C) Arp2/3/Cort, (D) Arp2/3/Cort+PI(5)P (67 mM), (E) Arp2/3/Cort+PI(5)P (100 mM), (F) Arp2/3/Cort+PI(4)P (67 mM)

<u>Task 2: Determine whether the interaction of cortactin with PI-3-P and PI-5-P is required for cell migration and tumor metastasis</u>

While the previous study has shown that certain types of phospholipids such as PI(4)P can inhibit the activity of cortactin, we have not yet been able to finish the characterization of the motif for PI(4) binding during the funding period. This was partially due to the changes of laboratory personals as the result of the recent shout down of the Holland Laboratory of ARC.

However, other studies that was also supported this grant have yielded many significant results (see the list of our recent publications). The most significant result is that we have found that cortactin binds to the gene product of missing in metastasis (MIM), which is

frequently silent in many invasive tumor cells. Binding to MIM is apparently regulated by extracellular stimuli including FGF and PDGF in a Src dependent manner. More significantly, MIM enhances the cortactin mediated actin polymerization. Interestingly, overexpression of MIM results in inhibition of cell migration induced by PDGF. This new finding indicates a novel signal pathway from growth factors to cell migration, an perhaps metastasis. Details for this finding can be found in the attached two manuscripts (11, 12). Future study will be directed to reveal the potential role of this new pathway in tumor metastasis.

Key research accomplishments

1. Established the method to prepare liposomes and analyze the activity of phospholipids in actin assembly.

2. Demonstrated that PI(4) can inhibit cortactin mediated actin polymerization

3. Discovered that cortactin binds to MIM and demonstrated that MIM regulates the cortactin mediated actin polymerization

Reportable outcomes

1. Li Y, Tondravi M, Liu J, Smith E, Haudenschild CC, Kaczmarek M, Zhan X. Cortactin potentiates bone metastasis of breast cancer cells. Cancer Res 2001;61:6906-6911.
2. Dudek SM, Birukov KG, Zhan X, Garcia JG. Novel interaction of cortactin with endothelial cell myosin light chain kinase. Biochem Biophys Res Commun 2002;298:511-519.
3. Di Ciano C, Nie Z, Szaszi K, Lewis A, Uruno T, Zhan X, Rotstein OD, Mak A, Kapus A. Osmotic stress-induced remodeling of the cortical cytoskeleton Am J Physiol Cell Physiol 2002; 283: 850-865
4. Uruno T, Zhang P, Liu J, Jian-Jiang H, Zhan X. Hemaptopietic lineage cell specific protein 1 (HS1) promotes the Arp2/3 complex-mediated actin polymerization. Biochem J 2003; 371, 485-493.
5. Uruno T., Liu, J., Li, Y., Smith, N., Zhan X. Sequential interaction of Arp2/3 complex with N-WASP and cortactin during branched actin filament network formation. J. Biol. Chem. 2003; 278: 26086-26093.
6. Van Rossum, A. G., De Graaf, J. H., Schuuring-Scholtes, E., Kluin, P. M., Fang, Y. X., Zhan, X., Moolenaar, W. H., and Schuuring, E. Alternative splicing of the actin-binding domain of human cortactin affects cell migration. J.Biol.Chem., 2003. 278: 45672-45679
7. Dudek, S.M., J.R.Jacobson, E.T.Chiang, K.G.Birukov, P.Wang, X.Zhan, and J.G.Garcia. 2004. Pulmonary endothelial cell barrier enhancement by sphingosine 1-phosphate: Roles for cortactin and myosin light chain kinase. J. Biol. Chem. 279:24700.
8. Li, Y., T.Uruno, C.C.Haudenschild, Deudek, SM, J.Garcia, and X.Zhan. 2004. Interaction of cortactin and Arp2/3 complex is required for sphingosine-1-phosphate induced endothelial cell remodeling. Experimental Cell Research 298:107-121.
9. Hao, J. J. and Zhan, X. Tyrosine phosphorylation is required for the association of HS1 with lipid rafts and BCR signalosome complex. J. Biol. Chem. 2004 (in press).
10. Zhu, J. Zhou, K.; Liu, J.; Hao, J., and Zhan, X. Regulation of the interaction between dynamin and cortactin by Arp2/3 complex mediated actin polymerization during the fission of clathrin coated pits (submitted)
11. Lin X, Y.Wang, J.Liu, Smith N., and X.Zhan. Differntial regulation of cortactin and N-WASP mediated actin polymerization by missing in metastasis (MIM) protein. 2004a. (submitted)
12. Lin X, Y.Wang, J.Zhu, H.Zhou, J.Liu, Smith N., Y.Li, and X.Zhan. Src-mediated association of missing in metastasis (MIM) with cortactin links platelet derived growth factor signal transduction to actin cytoskeleton. 2004b. (submitted)

Conclusions

1. Different types of phospholipids exhibit different specific activity on cortactin. PI(4)P inhibits cortactin while PI(5)P enhances the activity of cortactin.

2. Cortactin is essential for the formation of invadopodia of breast cancer cells.

3. MIM is a cortactin binding protein and regulates cortactin mediated cell motility

4. Overexpression of MIM inhibits cell motility

Personal list:

Li, Yansong
Hao, Jin-Jiang
Liu, Jiali
Smith, Nicole
Wang, Ying
Zhou, Hong
Zhou, Kang
Zhu, Jian-Wei

Appendices

<u>Submitted manuscripts.</u>

Lin X, Y.Wang, J.Liu, Smith N., and X.Zhan. Differntial regulation of cortactin and N-WASP mediated actin polymerization by missing in metastasis (MIM) protein. 2004.

Lin X, Y.Wang, J.Zhu, H.Zhou, J.Liu, Smith N., Y.Li, and X.Zhan. Src-mediated association of missing in metastasis (MIM) with cortactin links platelet derived growth factor signal transduction to actin cytoskeleton. 2004

Differential regulation of cortactin and N-WASP mediated actin polymerization by missing

in metastasis (MIM) protein

Jinxiu Lin[2]† Jiali Liu[1] , Ying Wang[1], Janwei Zhu[1], Kang Zhou[1], Nicole Smith[2] and Xi Zhan[1*]

[1] Greenebaum Cancer Center, Department of Pathology,
University of Maryland School of Medicine, Baltimore, Maryland

[2]Holland Laboratory,
American Red Cross
15601Crabbs Branch Way
Rockville, Maryland 20855

†Current address: Department of Cardiology,
First Affiliated Hospital of Fujian Medical University,
Fuzhou 350005, China

*Corresponding author
Telephone: (301) 738-0568

Fax: (301) 517-0352

E-mail: szhan001@umaryland.edu

Running title: MIM activates cortactin

Key words: MIM, cortactin, N-WASP, actin, cell motility, PDGF

Abstract

Missing in metastasis (MIM) gene encodes a protein that contains a WH2 domain, which binds to globular (G)-actin, and is expressed at low levels in a subset of malignant cell lines. MIM protein tagged by green fluorescent protein (GFP) colocalizes with cortactin, an Arp2/3 complex activator, and interacts directly with the SH3 domain of cortactin. Recombinant full-length MIM promotes markedly cortactin and Arp2/3 complex mediated actin polymerization in an SH3 dependent manner. In contrast, MIM-CT, a short splicing variant of MIM, is unable to enhance cortactin mediated actin polymerization and binds poorly to cortactin in vitro. Full length MIM also binds to G-actin with a similar affinity as N-WASP-VCA, a constitutively active form of N-WASP, and inhibits N-WASP-VCA mediated actin polymerization as analyzed in vitro. The significance of the association of MIM with cortactin and G-actin was evaluated in NIH3T3 cells expressing MIM mutants. Overexpression of full-length wild type MIM tagged by green fluorescent protein (GFP) inhibited markedly the motility of NIH 3T3 cells induced by PDGF and that of human vein umbilical endothelial cells induced by sphingosine 1 phosphate. However, a MIM mutant with deletion of the WH2 domain enhanced cell motility. The inhibitory activity of MIM was abolished in the cells overexpressing N-WASP. In contrast, deletion of MIM proline rich domain, which is required for an optimal binding to cortactin, substantiated the MIM-mediated inhibition of cell motility. These data imply that MIM regulates cell motility by modulating different Arp2/3 activators in a distinguished manner.

1

Introduction

Actin polymerization plays a pivotal role in cell migration, polarization, cytokinesis, cell adhesions and shape changes, and is ultimately implicated in a variety of stages of tumor progression, in particular, metastasis. In mammalian cells, two types of actin filaments have been described with each showing distinct physiological functions. One type is branched actin filaments that are normally associated with cortical areas such as lamellipodia or membrane ruffles, the structures that are responsible for membrane protrusions and cell migration (Mullins et al. 1998; Borisy and Svitkina 2000). The other type is nonbranched actin filaments such as stress fibers that are frequently associated with focal adhesions, adherent junctions and filopodia. The assembly of each type of actin filaments is directed by distinct cellular machineries. Branched actin filaments are nucleated by Arp2/3 complex (Pollard et al. 2000), whereas nonbranched actin filaments in focal adhesions and adherent junctions are assembled by formin family proteins (Evangelista et al. 2003). The Arp2/3 complex mediated actin assembly involves an activation step, which requires the function of WASP family proteins and cortactin. WASP related proteins are the targets of small GTPases such as Rac or Cdc42 (Pollard and Borisy 2003), whereas cortactin is the prominent substrate of Src protein tyrosine kinases (Wu and Parsons 1993; Zhan et al. 1993) and implicated in metastasis (Li et al. 2001). In the presence of both cortactin and WASP proteins, cortactin facilitates the release of activated WASP proteins from Arp2/3 complex at branching sites, promotes and stabilizes branched actin filaments (Uruno et al. 2003; Weaver et al. 2001).

MIM is a putative metastatic suppressor and expressed at low levels in a subset of highly invasive tumor cells (Lee et al. 2002). The predicted amino acid sequence of MIM encodes a protein that contains multiple function motifs, including a coiled-coil domain, a lysine rich

domain (LRD), serine rich domain (SRD), proline rich domain (PRD) and a WH2 domain at its C-terminus (Figure 1). MIM also shares a certain homology with insulin receptor substrate p53 (IRSp53) in a region of 250 amino acids at the N-terminus (Yamagishi et al. 2004). Studies with a short form of MIM protein containing the PRD and the WH2 domain demonstrated that MIM binds preferentially to the ATP bound G-actin (Mattila et al. 2003), and modulates negatively the rate of spontaneous actin polymerization in vitro (Mattila et al. 2003; Woodings et al. 2003), presumably by sequestration of the G-actin available for actin assembly. However, the intrinsic physiological function of MIM is still unknown as a technical difficulty to obtain recombinant full-length MIM protein (Mattila et al. 2003; Woodings et al. 2003). In this study, we found that MIM-GFP colocalizes with cortactin and interacts directly with the cortactin SH3 domain. Having successful preparation of recombinant full-length protein, we also demonstrated that MIM activates markedly cortactin but attenuates N-WASP mediated actin polymerization. Furthermore, we found that overexpression of MIM inhibits cell motility in a manner depending on interaction with cortactin and G-actin. Therefore, this study suggests that MIM may be implicated in cell motility by modulating different actin polymerization factors.

Results

MIM binds to cortactin by targeting to cortactin SH3 domain

To examine the physiological function of MIM, we prepared a DNA fragment encoding a full-length murine MIM protein in retroviral vector MGIN, in which MIM was tagged by GFP at its C-terminus (Cheng et al. 1997). Infection of the virus into NIH3T3 cells resulted in over 90% of cell population expressing MIM-GFP based on microscopic inspection (data not shown). In the examination of 3T3 cells overexpressing MIM-GFP, we noticed that MIM-GFP displayed frequently a punctate staining in the cytoplasm, the pattern that is similar to that of cortactin ((Liu et al. 1999)). Indeed, staining of cells with cortactin and GFP antibodies demonstrated that many MIM-GFP puncta were colocalized with cortactin (Figure 2A-C). To verify the direct interaction between cortactin and MIM, the lysates of cells expressing MIM-GFP were subjected to immunoprecipitation with GFP-antibody followed by immunoblot with cortactin antibody. This analysis showed that cortactin was readily precipitated in the immuno pellet (Figure 2E, left panel). Furthermore, cortactin antibody was also able to precipitate MIM-GFP (Figure 2E, right panel), but not GFP (data not shown).

The direct interaction between cortactin and MIM-GFP was further verified by pull down analysis using GST-cortactin (Figure 2D, lane 3). To examine the sequence of cortactin responsible for the interaction between cortactin and MIM-GFP, GST-CortΔSH3 and GST-Cort-SH3 proteins were also used to pull down MIM-GFP. While GST-Cort-SH3 was able to pull down readily MIM-GFP (lane 2), GST-CortΔSH3 failed to do so (lane 1). Furthermore, MIMΔPRD-GFP, a mutant with deletion of the sequence from 612 to 727 that contains three proline rich stretches, is required for optimal interaction between cortactin and MIM (Figure 2F).

4

Taken together, these data demonstrate that the interaction between cortactin and MIM occurs between the cortactin SH3 domain and a proline rich sequence of MIM.

MIM enhances cortactin mediated actin polymerization

To evaluate the biochemical function of MIM, we made an effort to prepare full length murine MIM proteins tagged by either 6 x His or GST epitope in bacterial strain BL21-CodonPlus-RPLI, which contains extra copies of Arg, Pro, and Leu tRNA genes, as the host for MIM. The rationale to use this host is that Arg, Pro and Leu residues are apparently over represented in the predicted MIM amino acid sequence and may quickly exhaust the limited pool of their corresponding tRNAs in common *E. Coli* strains, resulting in lower level of expression (Makrides 1996). With this system, we were able to prepare soluble His-MIM or GST-MIM proteins with purity over 90%. On SDS-PAGE, His-MIM migrates at a position with an apparent molecular weight of 120 kDa (Figure 1B), which is significantly larger than 80 kDa as predicted from a full length cDNA, indicating that MIM may have an irregular configuration. Consistent with this, MIM-GFP expressed in cells also displays an apparent molecular weight of 150 kDa (Figure 2E), which is greater than predicted 110 kDa.

To explore the functional significance of the interaction between MIM and cortactin, we evaluated the potential effect of His-MIM on the cortactin mediated polymerization of pyrene labeled G-actin as described previously (Uruno et al. 2001). In the presence of 100 nM cortactin and 100 nM Arp2/3 complex, approximately 300 sec was required to reach a half maximal actin polymerization. In contrast, the same level of actin assembly was achieved within 95 sec when 10 nM His-MIM was added. A further time course analysis of the half maximal stimulation ($t_{1/2}$) demonstrated that His-MIM was able to activate cortactin maximally at concentrations as low as 2 nM (Figure 3C). Interestingly, His-MIM started to inhibit actin assembly at higher

concentrations, suggesting that His-MIM may be able to sequestrate G-actin, a property shared by many G-actin binding proteins (Bubb et al. 1991; Safer et al. 1991). Indeed, when His-MIM was evaluated in the absence of Arp2/3 complex and cortactin, it inhibited the rate of actin polymerization in a dose dependent manner (Figure 3C). At 800 nM, actin polymerization was nearly abolished. This inhibitory activity is similar to that of MIM-CT as previously described (Woodings et al. 2003; Mattila et al. 2003).

The role of the interaction between cortactin and MIM was evaluated with CortΔSH3, which was unable to bind to MIM (Figure 2D). As shown in Figure 4A, His-MIM failed to enhance the activity of CortΔSH3 within the concentration ranges in which it activated significantly wild type cortactin (Figure 3B). Thus, direct binding to cortactin is necessary for MIM to activate cortactin.

Activation of cortactin mediated actin polymerization requires full-length MIM

To examine whether the binding to the SH3 domain would be sufficient for MIM to activate cortactin, we analyzed the effect of His-MIM-CT, a short splicing variant of MIM that has been previously studied, on the cortactin mediated actin polymerization. Unlike full-length MIM, His-MIM-CT showed no ability to promote the cortactin/Arp2/3 mediated actin polymerization at concentrations ranging from 10 to 100 nM (Figure 4B). However, it started to inhibit the actin polymerization at the concentration over 200 nM.

Inability of His-MIM-CT to activate cortactin implied that binding to cortactin requires full length of MIM. Indeed, a quantitative analysis of the interaction between His-MIM-CT and His-cortactin demonstrated that His-MIM-CT binds to cortactin with an equilibrium dissociation constant (Kd) of 3770 nM, whereas His-MIM has a Kd of 440 nM (Figure 4C). Thus, His-MIM-CT is a poor cortactin binding protein.

MIM inhibits N-WASP mediated actin polymerization in a G-actin binding dependent manner

WASP and its related molecules are a protein family that activate Arp2/3 complex through their ability to recruit G-actin to the complex (Pollard and Borisy 2003). N-WASP-VCA, a constitutively activated form of N-WASP, stimulates potently Arp2/3 complex mediated actin polymerization (Egile et al. 1999). In the presence of 100 nM Arp2/3 complex and 5 nM N-WASP-VCA, His-MIM reduced significantly actin assembly at a concentration as low as 10 nM (Figure 5A). At 60 nM, the rate of actin polymerization was reduced to a level close to that of actin alone. When a higher concentration (10 nM) of N-WASP-VCA was used, 200 nM His-MIM was needed to abolish the actin assembly (data not shown).

Because both MIM and N-WASP-VCA contain a WH2 domain, which is a G-actin binding motif, we assumed a possible competition between N-WASP-VCA and MIM for G-actin. Indeed, both N-WASP-VCA and His-MIM bound to G-actin effectively with an affinity of 78.2 nM and 94.0 nM, respectively (Figure 5B). Furthermore, MIM mutant with deletion of the WH2 domain did not inhibit but actually enhanced slightly actin assembly at concentrations of 5 and 10 nM (Figure 5C).

MIM modulates the agonist-induced cell motility in a manner depending on its interaction with cortactin and G-actin

The function of MIM in actin assembly implied that MIM may be involved in cell motility. Therefore, we examined the motility of NIH3T3 cells expressing MIM-GFP or GFP as analyzed by Transwell, a modified Boyden chamber, under a condition with or without PDGF stimulation. In the absence of PDGF, no apparent difference in migration through Transwell was observed between the cells overexpressing MIM-GFP and the cells expressing GFP only (Figure

6A). However, the cells overexpressing MIM-GFP showed a significant lower motility in response to PDGF than the control cells. PDGF stimulation resulted in approximately 100% increase in the motility of control cells but only about 20% of the cells expressing MIM-GFP (Figure 6A). In addition to NIH3T3 cells, we also examined the motility of human umbilical vein endothelial cells (HUVEC) infected with MIM-GFP viruses in response to sphingosine 1 phosphate (S1P), a potent chemotactant that triggered about 2-fold increase in the motility of HUVE cells expressing GFP alone (Figure 6B). However, S1P induced only 50% increase in the motility of the cells overexpressing MIM-GFP. Again, no significant difference was observed when the motility of cells expressing MIM-GFP and GFP alone was compared in the absence of S1P. Thus, overexpression of MIM antagonizes specifically extracellular stimuli induced cell motility.

To evaluate the role of the interaction between cortactin and MIM in cell motility, we examined the motility of NIH3T3 cells expressing a MIM mutant MIMΔ(612-727)-GFP, which is deficient in cortactin binding. As shown in Figure 4C and 4D, the cells expressing the mutant migrated less efficiently compared to control cells expressing GFP alone or the cells expressing MIM-GFP under the condition without PDGF treatment. More significantly, the cells responded poorly to PDGF for cell migration. On the basis of the ratio of the motility in the presence of PDGF to that in the absence of PDGF, the cells expressing MIM-GFP and GFP alone showed 40% and 110% response to PDGF, respectively, while the mutant overexpressors had only approximately 8% response (Figure 6D). Thus, binding to cortactin substantiated the cell motility.

We also analyzed the motility of the cells expressing MIMΔWH2-GFP mutant, which does not bind to G-actin and is not able to interfere with N-WASP mediated actin polymerization (Figure 5C). Interestingly, these cells showed a 37% higher motility than the GFP expressing

8

cells under the condition with or without PDGF treatment (Figure 6D), resulting in an apparent similar motility response to PDGF (Figure 6D). The difference was even greater when compared to the motility of the cells expressing MIM-GFP. The cells expressing the mutant migrated at a rate ~40% higher than the cells expressing MIM-GFP in the absence of PDGF, and ~100% higher in the presence of PDGF.

To confirm whether or not the apparent lower motility of the cells overexpressing MIM-GFP was due to inhibition of the function of N-WASP, NIH 3T3 cells were co-infected by viruses encoding N-WASP-GFP and MIM-GFP. The infected cells were then subjected to motility analysis. While the cells overexpressing N-WASP-GFP did not show increase in PDGF induced motility (Figure 6F), co-expression of N-WASP-GFP and MIM-GFP showed a similar motility response to PDGF as the control cells. Thus, overexpression of N-WASP-GFP rescued MIM mediated inhibition of cell motility.

Discussion

In this study, we provided evidence for the first time that full-length MIM has a dual function to modulate different types of Arp2/3 activators. It activates cortactin but antagonizes N-WASP mediated actin polymerization as analyzed in vitro. However, overexpression of MIM inhibited the motility of NIH3T3 and HUVE cells induced by their agonists, suggesting that the MIM induced cortactin activation is overshadowed by its attenuation of N-WASP at least in overexpressing cells. Consistent with the suppression of the function of N-WASP, MIM mediated cell motility inhibition was attenuated in the cells overexpressing N-WASP-GFP. Inhibition of N-WASP-VCA by MIM as manifested in vitro is likely due to a competition for G-actin because VCA and MIM have a very similar affinity for G-actin (Figure 5B). Furthermore, a MIM mutant with deletion of the WH2 domain failed to inhibit N-WASP-VCA in vitro and cell motility in vivo (Figure 5C). In fact, the rate of actin polymerization was slightly enhanced in the presence of the mutant without the WH2 domain at low concentrations. The reason for the enhancement is unclear. It may be due to other activities associated with different domains. Indeed, MIM also shows a strong affinity for F-actin as analyzed in vitro (data not shown), the property that may stabilize nascent actin filaments at low concentrations. The same F-actin binding activity could also explain a slight inhibitory activity of the mutant at high concentrations (greater than 60 nM) as shown in Figure 5C because the activity could prevent Arp2/3 complex from F-actin binding, which is essential for actin nucleation. Although our presented data suggest that N-WASP is a target of MIM in cells, MIM may also attenuate other WASP related proteins such as WAVE/Scar proteins, which also contain a WH2 domain (Millard et al. 2004). Determination of the intrinsic target of MIM in cells will require further efforts to dissect the specific role of MIM in the function of each member of the WASP family.

MIM mediated cortactin activation appears to be dependent upon its ability to interact directly with the cortactin SH3 domain because it has no influence on a cortactin mutant without the SH3 domain (Figure 4A). While this result indicates that binding to the SH3 domain would be necessary for the activation of cortactin mediated actin polymerization, other data suggest that it is unlikely the sole mechanism. In fact, GST tagged PRD motif of dynamin 2, which has a comparable affinity for cortactin as MIM, is unable to enhance the cortactin mediated actin assembly (data not shown). Previous studies have shown that WIP, dynamin 2 and Fdg1, all of which contain a PRD and are able to bind to the cortactin SH3 domain, display a certain activity to promote the cortactin mediated actin polymerization in vitro (Kinley et al. 2003; Schafer et al. 2002; Kim et al. 2004b). However, the extent to which these proteins activate cortactin is significantly different. Dynamin 2 mediated cortactin activation appears to be very modest. Based on the time to induce a half maximum of actin assembly, dynamin 2 induces a less than 30% increase in the cortactin activity under an optimal condition (Schafer et al. 2002). In the case of Fdg1, a peptide of Fdg1-PRD itself is unable to activate cortactin. However, a GST-Fdg1-PRD fusion protein shows a potential to activate cortactin in an efficiency similar to dynamin 2 (Kim et al. 2004a). Because GST is known to form a stable dimer (Weiss et al. 1992), the apparent effect of GST-Fdg1-PRD was thought to be the result of a possible dimerization of cortactin induced by the GST fusion. We have frequently observed that cortactin mutant with deletion of the SH3 domain showed a slight increase (~30%) as compared to wild type cortactin (Figure 4A, data not shown), suggesting that the SH3 domain may impose a weak self-inhibition to the function of cortactin. Therefore, it is more likely that dynamin 2 or GST-Fdg1-PRD promotes the cortactin's activity simply by blocking this potential autoinhibition on the SH3 domain. In contrast, MIM induced cortactin activation is quite substantial because it is able to

enhance cortactin mediated actin polymerization by more than 3-fold (Figure 3A). This suggests that MIM may activate cortactin by a mechanism(s) involving other functions that need to be further characterized. One possible function is that full length MIM has an F-actin binding activity, which may facilitate cortactin mediated actin polymerization. Consistent with this view, WIP, which is able to activate cortactin by nearly 2-folds (Kinley et al. 2003), also shows an F-actin binding activity (Martinez-Quiles et al. 2001).

Full-length MIM also differs from MIM-CT at its binding to cortactin and activation of cortactin mediated actin polymerization. Although MIM-CT contains a PRD for cortactin, His-MIM-CT binds to cortactin poorly with a Kd of 3.7 μM (Figure 4C) and is unable to precipitate cortactin in a convenient pull down assay (data not shown). Interestingly, MIM-CT tagged by GST binds strongly to cortactin with an affinity of 1.1 μM and is able to pull down readily cortactin (data not shown). This suggests that His-MIM-CT may not be correctly folded with respect to the function of PRD. One possibility is that the correct folding of MIM requires dimerization because GST is a dimmer. While it is unclear whether full-length MIM also assumes a dimeric form, our data indicates that working on a full-length form is necessary to characterize the complete function of MIM. It is interesting to note that His-MIM-CT is still able to inhibit actin polymerization at high concentrations, indicating that its WH2 domain, which locates at the C-terminus, is functional. Since His-MIM-CT is a short splicing variant, the isoform may acquire a unique function that interferes with specifically WASP related proteins. Whether or not MIM-CT is ever expressed within cells requires further investigation.

Figureure Legends

Figure 1. Schematic presentation of MIM, MIM-CT and other MIM constructs. IMD: IRsp53 and MIM homology domain; CC, coiled-coil domain; LRD: Lysine rich domain; SRD, serine rich domain; PRD, proline rich domain; and WH2, WASP homology 2 domain.

Figure 2. MIM associates with cortactin. NIH3T3 cells expressing MIM-GFP grown on fibronectin coated glass cover slips were stained with polyclonal GFP antibody (**A**) and monoclonal cortactin antibody (**B**) The cells were inspected under a fluorescent microscope using a 60 x oil lens. The cell digital images were captured and further processed by Adobe Photoshop. (**C**) The merged images of A and B. (**D**) Analysis of the interaction between cortactin with MIM. Left panel, NIH3T3 cells expressing MIM-GFP or GFP only were immunoprecipitated with polyclonal GFP antibody. The pellets were separated by SDS-PAGE and then immunoblotted with cortactin monoclonal antibody 4F11 (upper panel). The same blot was stripped and reblotted with GFP antibody to confirm the expression of MIM-GFP (lower panel). Right panel, the above cell lysates were immunoprecipitated first with polyclonal cortactin antibody and the pellets were fractionated by SDS-PAGE, transferred to a membrane and analyzed for the presence of MIM-GFP by immunoblot using GFP antibody. The same membrane was also blotted with cortactin antibody. (**E**) Pull down analysis of interaction between cortactin and MIM. GST conjugated proteins (5 µg) were mixed with lysates of 3T3 cells (1×10^6) expressing MIM-GFP and glutathione Sepharose beads. After precipitation, the pellets were washed three times, fractionated by SDS-PAGE followed by immunoblot with GFP antibody. Lane 1, GST-CortΔSH3; lane 2, GST-Cort-SH3; and lane 3, GST-cortactin. The position of MIM-GFP was indicated by an arrow. (**F**) MIM PRD is necessary for binding to cortactin. GST-Cort-SH3 was used to pull down the lysates from NIH3T3 expressing MIM-GFP

13

and MIMΔPRD-GFP. The pellet was immunoblotted with anti-GFP antibody (upper panel). Lower panel, immunoblot of total cell lysates of 3T3/MIM-GFP and 3T3/MIMΔPRD-GFP cells, showing relative expression levels of each protein.

Figure 3. MIM enhances cortactin mediated actin polymerization. (**A**) Commassie staining of SDS-PAGE containing purified His-MIM and His-cortactin. Mouse full length MIM was expressed as 6 consecutive histidine residues (6×His) fusion protein in BL21-CodonPlus(DE3)-RIPL competent cells. Cells were grown in 2 liters of Luria broth medium to OD_{600}=0.6. Expression was induced by 0.6 mM isopropyl-β-D-1-thiogalactosidase and culture was incubated at 34°C for additional 2 h. Bacterial pellets were collected, resuspended in 30 ml lysis buffer (50 mM NaH_2PO_4, pH 8.0, 300 mM NaCl, 10 mM imidazole, 1 mM PMSF, and 0.2 mg/ml lysozyme), lysed by sonication, and centrifuged at 14,000 rpm for 20 min. His fusion proteins were isolated from the supernatant by incubation with 1.5 ml Ni-NTA beads (Qiagen). The beads were then washed three times with 50 mM NaH_2PO_4, pH 8.0, 300 mM NaCl, and 15 mM imidazole and packed in a plastic Poly-PreP chromatography column (Bio-Rad). His fusion proteins were eluted with 4 ml of elution buffer (50 mM NaH_2PO_4, pH 8.0, 300 mM NaCl and 100 mM imidazole). The eluted sample was exchanged to 50 mM Tris-HCl, pH 8.0 and 24 mM KCl by passing through a PD-10 column, further purified by Mono Q-Sepharose anion-exchange chromatography column in an HPLC system, and eluted with a linear gradient from 0.024 M to 1 M KCl. The peak fraction containing His-MIM was collected and dialyzed against 5 mM Tris-HCl, pH 8.0, and 50 mM KCl. His-cortactin was prepared as previously described (Uruno et al. 2003). (**B**) Polymerization of G-actin (10% pyrene-labeled) was initiated in the presence of Arp2/3 (100 nM), cortactin (100 nM) and His-MIM at concentrations as indicated. The increase of pyrene fluorescence was detected as previously described (Uruno et al. 2001). (**C**) Actin

polymerization was initiated as in A. His-MIM concentration used in the reaction was 0, 1, 2, 4, 6, 8, 10, 15 and 20 nM, respectively. The time ($t_{1/2}$) at which actin polymerization reached to half maximum was plotted as a function of His-MIM concentration. (**D**) Actin polymerization was conducted in the presence of pyrene-labeled G-actin and His-MIM without Arp2/3 complex.

Figure 4. Binding to SH3 domain is essential for MIM to activate cortactin. (**A**) Polymerization of pyrene labeled actin was performed under conditions: 100 nM Arp2/3, 100 nM CortΔSH3 and His-MIM at varying concentrations. (**B**) Polymerization of actin was performed under the condition: 100 nM Arp2/3, 100 nM cortactin and His-MIM-CT at varying concentrations. (**C**) Analysis of the affinity of MIM and MIM-CT for cortactin. Bead immobilized His-MIM or GST-MIM-CT (8 µg) were incubated for 2 h with cortactin at the concentrations as indicated. After brief centrifugation, aliquots of supernatants were subjected to SDS-PAGE followed by immunoblot using anti-cortactin monoclonal antibody 4F11 (lower panels). The blot was digitalized by film scanning and quantified by Scion Image software. The resulting digital data were used to fit a single rectangular hyperbola using Sigma Plot version 8.0, resulting in Kd values as indicated.

Figure 5. MIM inhibits N-WASP-VCA mediated actin polymerization. (**A**) Polymerization of pyrene-G-actin was initiated in the presence of Arp2/3 (100 nM) alone, or plus VCA (5 nM), or plus His-MIM at concentrations as indicated. (**B**) Comparison of the affinity of MIM and VCA for G-actin. G-actin (1.4 µM) was incubated with purified His-MIM or GST-VCA ranging from 0 to 1000 nM in the presence of either Ni-NTA beads or glutathione 4B beads at 4°C. After 2 h of incubation, the samples were centrifuged. G-actin in the supernatant was detected by SDS-PAGE followed by Commassie blue staining. The intensity of G-actin bands was quantified and

15

used to calculate Kd values. **(C)** WH2 domain is required for MIM to inhibit VCA mediated actin polymerization. The condition was the same as (A) except that His-MIMΔWH2 was used.

Figure 6. Overexpression of MIM inhibits cell motility induced by PDGF. (A) NIH3T3 cells expressing either MIM-GFP or GFP were grown to 70% confluence and serum-starved for overnight. The serum-starved cells were trypsinized, re-suspended in DMEM and plated on the upper side of fibronectin coated filters (pore size = 8 μm) in Transwell at a density of 3×10^4 cells/well. The lower chambers were filled with serum-free medium or the same medium containing PDGF (30 ng/ml). Cells were allowed to migrate for 6 h in a humidified incubator containing 5% CO_2 at 37°C. Non-migratory cells were removed from the top filter surface with a cotton swab. The cells migrated to the bottom surface were fixed in 4% paraformaldehyde in PBS for 30 min at room temperature, stained with Harris hematixylin modified solution for 30 min and viewed under a phase contrast microscope (200×magnification). For each sample, digital images of 5 random microscopic fields were taken by Nikon camera equipped on the microscope and the number of migrated cells was counted using MetaMorph 6.1 program. Relative cell motility of each sample was calculated by comparison to the motility of the cells expressing GFP alone. **(B)** HUVE cells expressing MIM-GFP or GFP were quiescent in a low serum medium and analyzed for cell motility as in A except M199 medium containing 0.5 μM S1P was used. **(C-E)** NIH3T3 cells infected with GFP, MIM-GFP, MIMΔPRD-GFP and MIMΔWH2-GFP viruses were analyzed for the motility response to PDGF as described in A. **C**, representative images of the cells on the lower side of the chamber; **D**, plot of the motility of each sample as in A; **E**, cell motility of each sample was represented as the ratio of the motility in the presence of PDGF to that without PDGF treatment. **(F)** NIH3T3 cells or cells expressing MIM-GFP were infected with a retrovirus encoding N-WASP-GFP. The infected cells were then

16

subjected to motility assay as in A and the PDGF stimulated motility was presented as in E. All the data were shown as the means $\pm$ S.D. of three independent experiments. *$p<0.01$ was calculated by paired t-test, referring to the difference between the indicated samples and the control sample (GFP).

Reference List

Borisy GG and Svitkina TM. (2000). *Curr Opin Cell Biol,* **12,** 104-112.

Bubb MR, Lewis MS and Korn ED. (1991). *J Biol Chem,* **266,** 3820-3826.

Cheng L, Du C, Murray D, Tong X, Zhang YA, Chen BP and Hawley RG. (1997). *Gene Ther,* **4,** 1013-1022.

Egile C, Loisel TP, Laurent V, Li R, Pantaloni D, Sansonetti PJ and Carlier MF. (1999). *J Cell Biol,* **146,** 1319-1332.

Evangelista M, Zigmond S and Boone C. (2003). *J Cell Sci,* **116,** 2603-2611.

Kim K, Hou P, Gorski JL and Cooper JA. (2004a). *Biochemistry,* **43,** 2422-2427.

Kim K, Hou P, Gorski JL and Cooper JA. (2004b). *Biochemistry,* **43,** 2422-2427.

Kinley AW, Weed SA, Weaver AM, Karginov AV, Bissonette E, Cooper JA and Parsons JT. (2003). *Curr Biol,* **13,** 384-393.

Lee YG, Macoska JA, Korenchuk S and Pienta KJ. (2002). *Neoplasia,* **4,** 291-294.

Li Y, Tondravi M, Liu J, Smith E, Haudenschild CC, Kaczmarek M and Zhan X. (2001). *Cancer Res,* **61,** 6906-6911.

Liu J, Huang C and Zhan X. (1999). *Oncogene,* **18,** 6700-6706.

Makrides SC. (1996). *Microbiol Rev,* **60,** 512-538.

Martinez-Quiles N, Rohatgi R, Anton IM, Medina M, Saville SP, Miki H, Yamaguchi H, Takenawa T, Hartwig JH, Geha RS and Ramesh N. (2001). *Nat Cell Biol,* **3,** 484-491.

Mattila PK, Salminen M, Yamashiro T and Lappalainen P. (2003). *J Biol Chem,* **278,** 8452-8459.

Millard TH, Sharp SJ and Machesky LM. (2004). *Biochem J,* **380,** 1-17.

Mullins RD, Heuser JA and Pollard TD. (1998). *Proc Natl Acad Sci U S A,* **95,** 6181-6186.

Pollard TD, Blanchoin L and Mullins RD. (2000). *Annu Rev Biophys Biomol Struct,* **29,** 545-576.

Pollard TD and Borisy GG. (2003). *Cell,* **112,** 453-465.

Safer D, Elzinga M and Nachmias VT. (1991). *J Biol Chem,* **266,** 4029-4032.

Schafer DA, Weed SA, Binns D, Karginov AV, Parsons JT and Cooper JA. (2002). *Curr Biol,* **12,** 1852-1857.

Uruno T, Liu J, Li Y, Smith N and Zhan X. (2003). *J Biol Chem,* **278,** 26086-26093.

Uruno T, Liu J, Zhang P, Fan Y, Egile C, Li R, Mueller SC and Zhan X. (2001). *Nat Cell Biol,* **3,** 259-266.

Weaver AM, Karginov AV, Kinley AW, Weed SA, Li Y, Parsons JT and Cooper JA. (2001). *Curr Biol,* **11,** 370-374.

Weiss S, Konig B, Morikawa Y and Jones I. (1992). *Gene,* **121,** 203-212.

Woodings JA, Sharp SJ and Machesky LM. (2003). *Biochem J,* **371,** 463-471.

Wu H and Parsons JT. (1993). *J Cell Biol,* **120,** 1417-1426.

Yamagishi A, Masuda M, Ohki T, Onishi H and Mochizuki N. (2004). *J Biol Chem.*

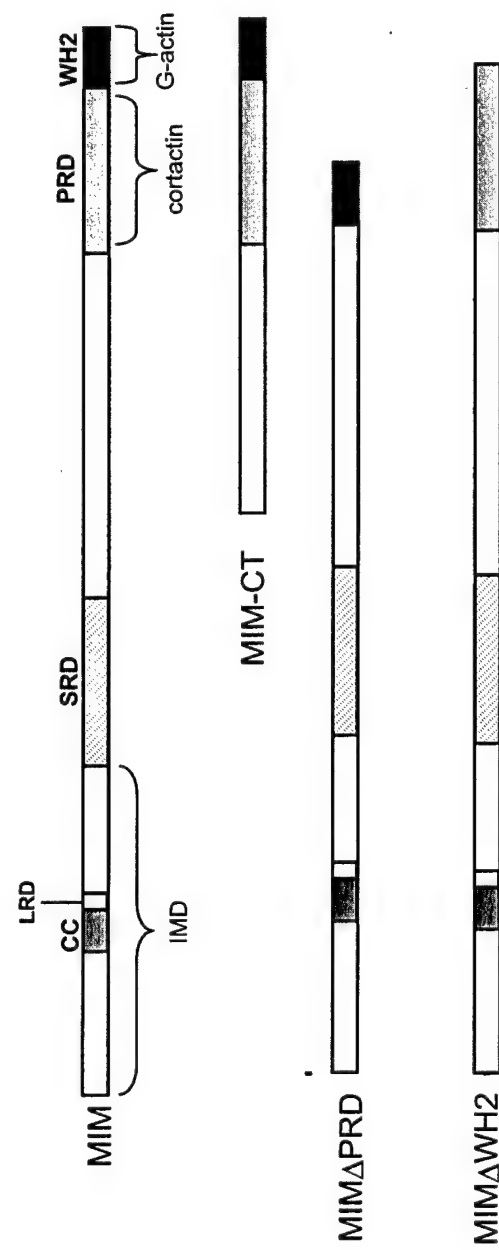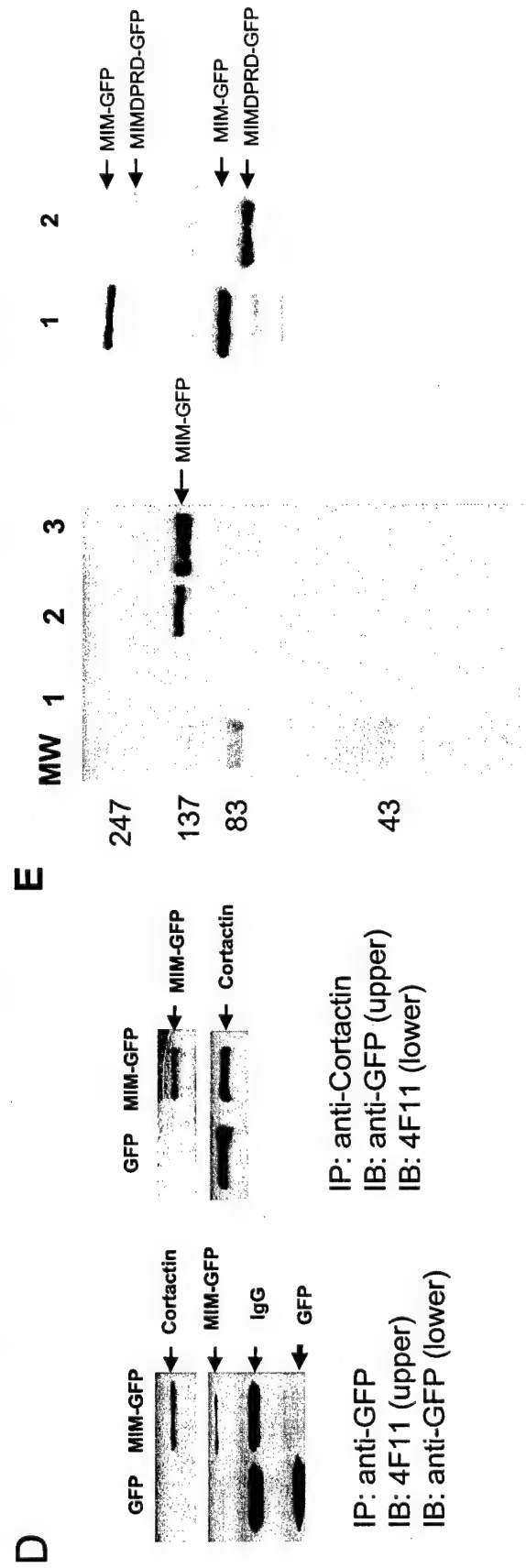Zhan X, Hu X, Hampton B, Burgess WH, Friesel R and Maciag T. (1993). *J Biol Chem,* **268,** 24427-24431.
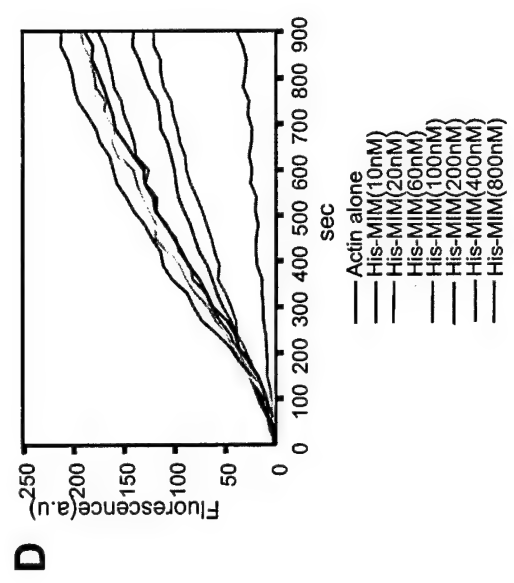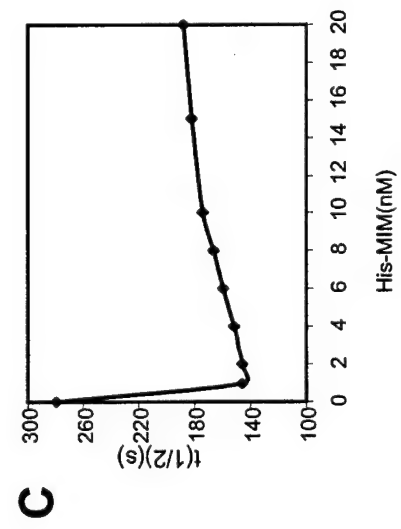
Fig 1

Fig 2

Fig 3

Fig 4

A

Fluorescence(a.u)

(1) Actin alone
(2) Arp2/3 (100nM)+CortΔSH3 (100nM)
(3) (2)+His-MIM(10nM)
(4) (2)+His-MIM(20nM)
(5) (2)+His-MIM(60nM)
(6) (2)+His-MIM(100nM)

B

Fluorescence(a.u)

(1) Actin alone
(2) Arp2/3 (100nM)+Cortactin(100nM)
(3) (2)+MIM-CT(10nM)
(4) (2)+MIM-CT(20nM)
(5) (2)+MIM-CT(60nM)
(6) (2)+MIM-CT(100nM)
(7) (2)+MIM-CT(200nM)

C

Depletion of MIM proteins (%)

$Kd_{His-MIM}=413$ nM

$Kd_{His-MIM-CT}=3770$ nM

Concentration (µM)

His-MIM
His-MIM-CT
GST-Cort (µM)   0   0.2 0.4 0.6 0.8 1.0 2.0

Fig 5

A

Fluorescence(a.u)

——(1) Actin alone
——(2) Arp2/3 (100nM)+VCA(5nM)
——(3) (2)+His-MIM(5nM)
——(4) (2)+His-MIM(10nM)
——(5) (2)+His-MIM(60nM)

sec

B

% depletion of actin

—— GST-VCA, Kd = 78.2 nM
—— His-MIM, Kd = 94.9 nM

(nM)

C

Fluorescence(a.u)

——(1) Actin alone
——(2) Arp2/3 (100nM)+VCA(5nM)
——(3) (2)+His-MIMΔWH2(5 nM)
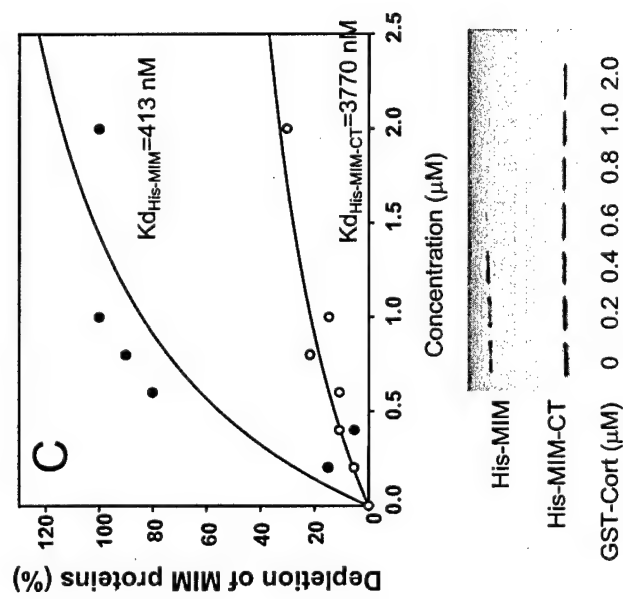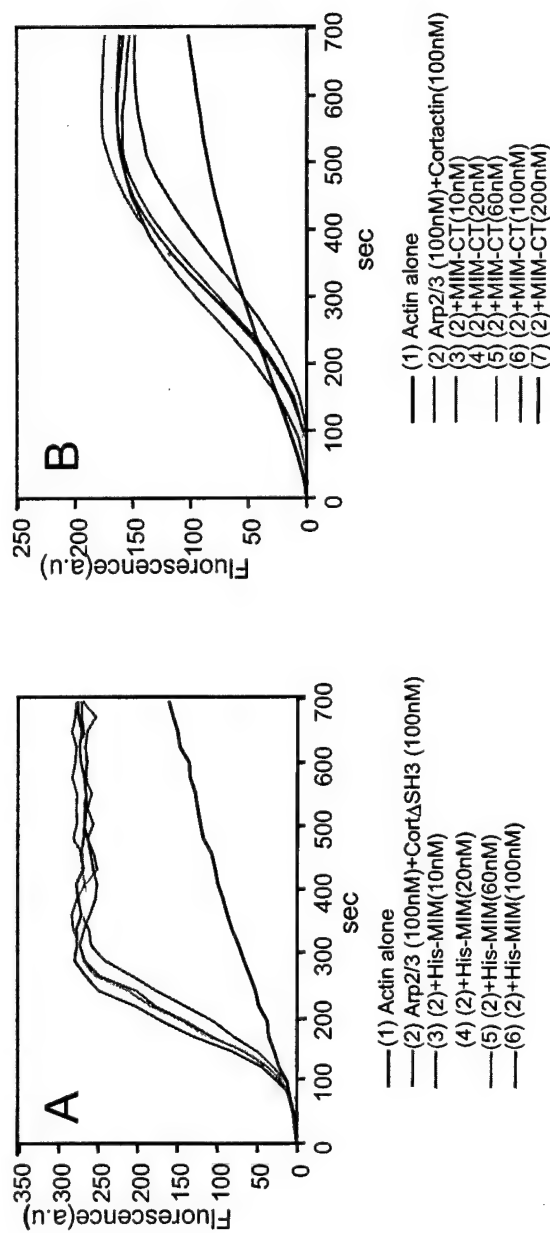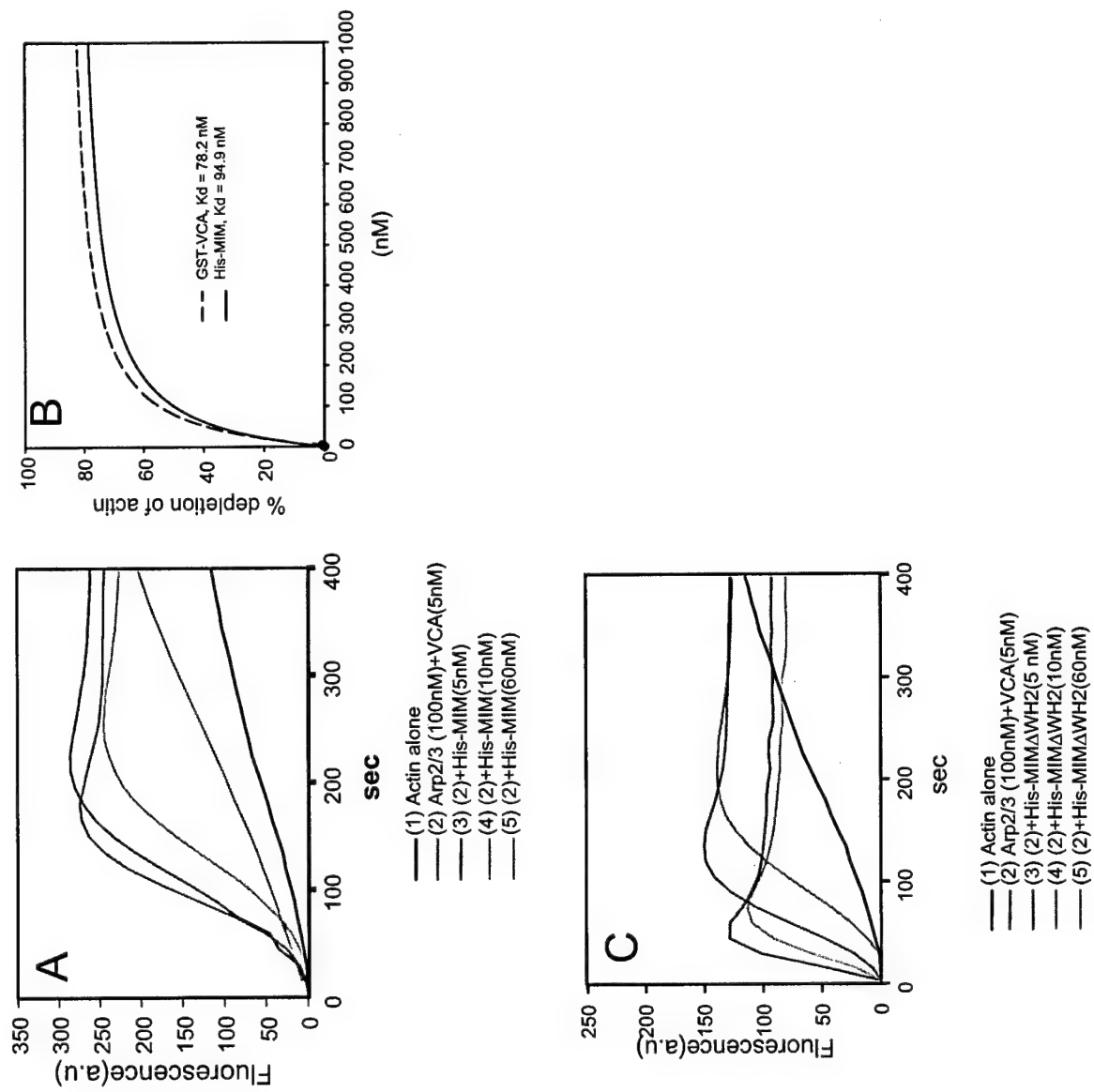——(4) (2)+His-MIMΔWH2(10nM)
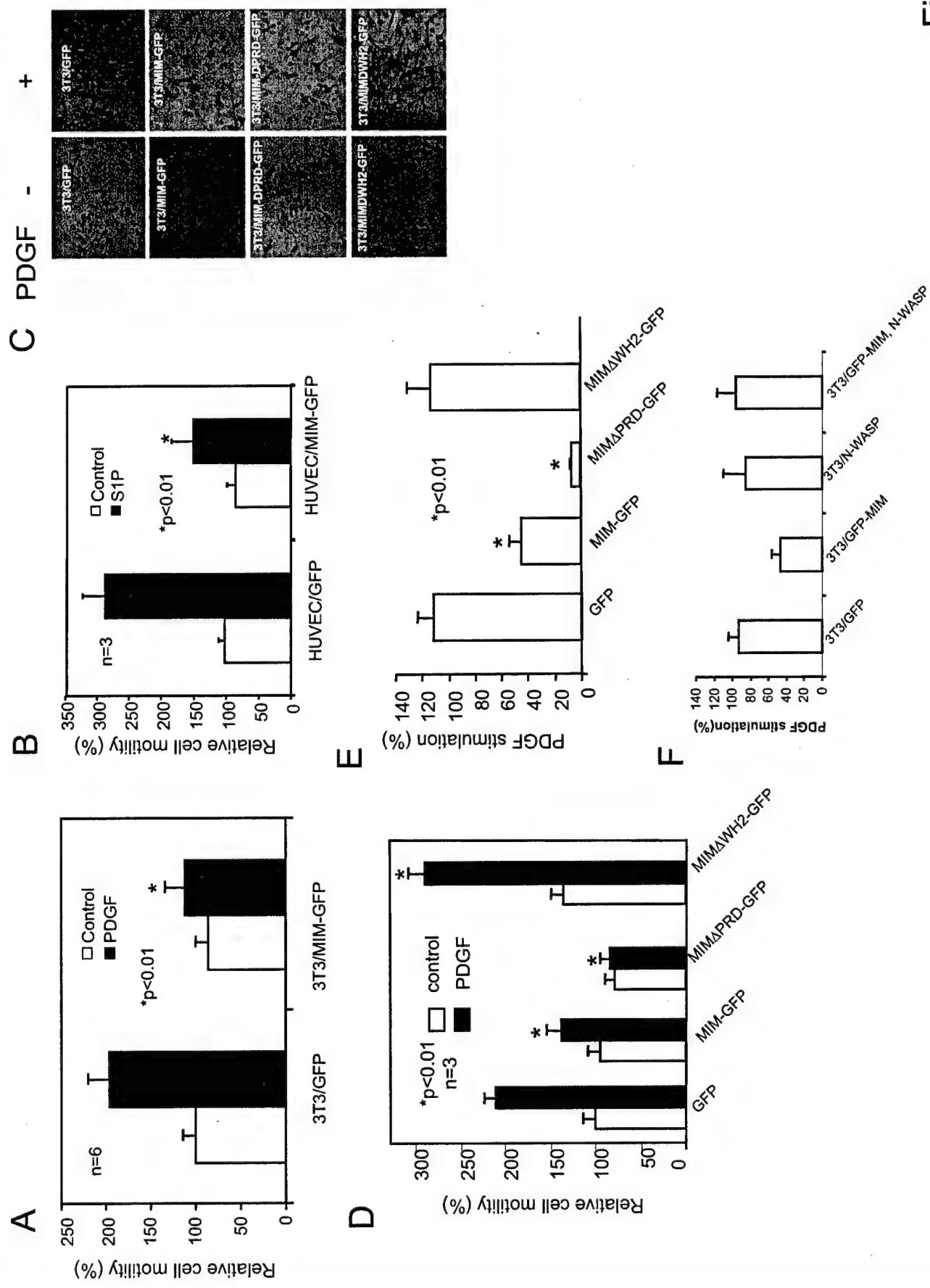——(5) (2)+His-MIMΔWH2(60nM)

sec

Fig 6

Src-mediated association of missing in metastasis (MIM) with cortactin links the platelet derived growth factor signal transduction to the actin cytoskeleton

Jinxiu Lin[1]†, Ying Wang[1,2], Jianwei Zhu[1,2], Hong Zhou[1], Jiali Liu[1,2], Nicole Smith[1], and Xi Zhan[1,2]*

[1]Holland Laboratory,
American Red Cross
15601Crabbs Branch Way
Rockville, Maryland 20855

[2]Greenebaum Cancer Center, Department of Pathology
University of Maryland School of Medicine

†Department of Cardiology,
First Affiliated Hospital of Fujian Medical University,
Fuzhou 350005, China

*Corresponding author
Telephone: (301) 738-0568

Fax: (301) 517-0352

E-mail: szhan001@umaryland.edu

Running title: Cortactin interacts with MIM

Key words: MIM, cortactin, Src, actin, PDGF

Abbreviations used: GFP, green fluorescent protein; GST, glutathione s-transferase; MIM, missing in MIM, PCR, polymerase chain reaction; PDGF, platelet derived growth factor; PRD, proline rich domain; and SH3, Src homology 3.

Abstract

Missing in metastasis (MIM) is a G-actin binding protein that is poorly expressed in a subset of malignant cells. Immunoprecipitation analysis demonstrated that MIM, as a GFP fusion protein expressed in NIH3T3 cells, interacts with cortactin, a substrate of Src and an activator of Arp2/3 complex for actin polymerization. Cell staining analysis revealed that MIM-GFP colocalized intimately with cortactin in many punctate structures of the cytoplasm. Interaction between MIM and cortactin requires the cortactin SH3 domain and a proline rich motif of MIM. Interestingly, coprecipitation of MIM-GFP and cortactin was dramatically enhanced from the lysates of cells that were treated with PDGF. In addition, MIM-GFP underwent a rapid tyrosine phosphorylation in NIH3T3 cells upon PDGF stimulation in a similar kinetics as the interaction with cortactin. However, PDGF induced tyrosine phosphorylation of MIM and interaction between MIM and cortactin were diminished in the cells treated with PP2, a selective inhibitor of protein tyrosine kinase Src. Furthermore, a cortactin mutant deficient in tyrosine phosphorylation associated poorly with MIM in PDGF treated cells. Thus, these data demonstrated for the first time that Src-mediated tyrosine phosphorylation regulates the interaction between cortactin and MIM, and indicated a new signaling pathway from growth factors to the actin cytoskeleton via phosphorylation of MIM.

Introduction

MIM was initially identified as a cDNA fragment encoding a protein of 356 amino acids (1). Because of its low expression in a subset of metastatic cells, it has been thought to act as a metastasis suppressor. Other studies further revealed the existence of longer cDNA clones of both human and mouse that encode a protein product with additional 403 amino acids at the N-terminus (2;3). The predicted full-length MIM protein contains multiple structural motifs, including a coiled-coil domain, a lysine rich domain (LRD), serine rich domain (SRD), proline rich domain (PRD) and a WH2 domain at its C-terminus (Figure 1A). MIM also shares a certain homology with insulin receptor substrate p53 (IRSp53) in a region of 250 amino acids at the N-terminus(4). Studies with a MIM variant (MIM-CT), which corresponds to the protein product of a short cDNA that contains the PRD and the WH2 domain only, demonstrated that MIM binds preferentially to the ATP bound G-actin (3) through its WH2 domain (2) and modulates negatively the rate of spontaneous actin polymerization in vitro (2;3). However, the intrinsic physiological function of MIM is still unknown because many G-actin binding proteins such as thymosin and actobindin also show a property to inhibit actin assembly by simply sequestration of the G-actin in the reaction (5;6). In particular, it has been a technical difficulty to obtain a recombinant full-length MIM protein and appropriate antibodies against MIM (2;3). Here, we provide evidence for the presence of full-length MIM protein in tissues and cells. We also report that MIM binds to cortactin, an intrinsic Arp2/3 complex binding protein that activates Arp2/3 mediated actin polymerization (7). Interestingly, the interaction between MIM and cortactin is not constitutive in the cell and is regulated in response to PDGF and requires the function of Src and tyrosine phosphorylation of cortactin. Hence, our data demonstrated a novel signaling

pathway from growth factors to the actin cytoskeleton via the interaction between MIM and cortactin.

Experimental Procedures

Reagents

All reagents, unless specially stated, were purchased from Sigma-Aldrich. (St. Louis). Protein A-Sepharose CL-4B and anti-His antibody were from Amersham Biosciences, Inc. (Piscataway). Monoclonal antiphosphotyrosine antibody (4G10), monoclonal anti-cortactin antibody (4F11) and anti-GST antibody were purchased from Upstate Biotechnology, Inc.(Lake Placid). Polyclonal and monoclonal anti-GFP antibody (11E5) were from Molecular Probes (Eugene). Polyclonal cortactin antibody was prepared as described previously (8).

Immunofluorescent microscopy

NIH-3T3 cells (1×10^5) infected with MIM-GFP viruses were seeded onto micro cover glasses pre-coated with fibronectin in a 12-well plate. After 24 h of serum starvation, cells were stimulated with PDGF (30 ng/ml) for 10 min. The cover glasses were washed twice with cold PBS and fixed with 4% paraformaldehyde in PBS for 30 min, permabelized in PBS containing 0.25% Triton X-100 for 2 min and incubated with polyclonal anti-GFP (4 µg/ml) and monoclonal cortactin antibody (1 µg/ml) for 1 h. The cell samples were washed three times with PBS and incubated with fluorescein isothiocyanate (FITC) conjugated goat anti-rabbit IgG and rhodamine conjugated goat anti-mouse IgG antibodies for 1 h. After three times of wash, the samples were mounted on a glass slide and inspected under a fluorescent microscope (Nikon TE2000U) using a 60 x oil lens. The cell images were captured by digital camera Nikon 1200F and further processed by Adobe Photoshop.

Plasmid preparation

Plasmids pHis-MIM, pGST-MIM and pGST-MIM-CT were prepared by polymerase chain reaction (PCR). Briefly, the full-length mouse MIM-GFP and GST-MIM-CT (the gifts of

Dr. Pekka Lappalainen, Institute of Biotechnology, University of Helsinki, Finland) were used as the template in PCR using CAGTGGCATATGGAGGCTGTGATCGAGAAG/ CAGTCGCTCGAGAGAGAAGCGCGGTGCTGA, TGATCAGGATCCGAGGCTGTGATCGAG/GACCTGGTCGACCTAAGAGAAGCGCGG, and GACCTGGGATCCTTCCCGTCATCTCAG/GACCTGGTCGACCTAAGAGAAGCGCGG as primers respectively. The resulting DNA products were inserted into the *Nde*1 and *Xho*1 sites of vector PET-23a to generate pHis-MIM, or *Bam*H1 and *Sal*1 sites of vector PGEX4T-2 to generate pGST-MIM and pGST-MIM-CT. Plasmid MGIN-MIM-GFP was prepared by cloning MIM-GFP into the *Sac*II and *Not*1 sites of retroviral vector MGIN. To generate MIMΔ(612-727)-GFP, deletion of amino acids 612-727 was prepared by PCR, and the DNA products were cloned into *Eco*R1 and *Not*1 sites of vector pEGFP-N1 for MIMΔ(612-727)-GFP.

Protein expression and purification

Mouse full length MIM was expressed as 6 consecutive histidine residues (6×His) fusion protein in BL21-CodonPlus(DE3)-RIPL competent cells (Stratagene) under the control of T7 lacUV5 promoter. Cells were grown in 2 liters of Luria broth medium at 37°C in a shaker at 200 rpm to an optical density of 0.6 at 600 nm. Expression was induced by adding 0.6 mM isopropyl-β-D-1-thiogalactosidase and incubated at 34°C. Cells were harvested 2 h after induction. Pellets were collected by centrifuging at 5,000 rpm for 20 min. Cell pellets were resuspended in 30 ml lysis buffer (50 mM NaH_2PO_4, pH 8.0, 300 mM NaCl, 10 mM imidazole, 1 mM PMSF, and 0.2 mg/ml lysozyme), placed on ice for 30 min, lysed by sonication (12 pulse cycles of 6 second-on and 6-second-off), and centrifuged at 14,000 rpm for 20 min. His fusion proteins were isolated from the supernatant by incubation with 1.5 ml Ni-NTA beads (Qiagen). The beads were then washed three times with 50 mM NaH_2PO_4, pH 8.0, 300 mM NaCl, and 15 mM imidazole. Beads

were packed in a plastic Poly-PreP chromatography column (Bio-Rad), and the His fusion proteins were eluted with 4 ml of elution buffer (50 mM NaH_2PO_4, pH 8.0, 300 mM NaCl and 100 mM imidazole). The eluted sample was exchanged to 50 mM Tris-HCl, pH 8.0 and 24 mM KCl by passing through a PD-10 column (Amersham Biosciences), further purified by Mono Q-Sepharose anion-exchange chromatography column (Amersham Biosciences) in an HPLC system (Waters), and eluted with a linear gradient from 0.024 M to 1 M KCl. The peak fraction containing His-MIM eluted at ~0.32 M KCl was collected and dialyzed against 5 mM Tris-HCl, pH 8.0, and 50 mM KCl. The purified protein was lyophilized and stored at -80°C. MIM-CT, cortactin, Arp2/3 and VCA were prepared as previously described (3;7). Protein concentration was determined by the Bradford method using BSA as the standard.

GST-MIM was prepared from the same bacterial strain as above and purified as described previously (9).

Antibody preparation

Purified GST-MIM protein was separated by SDS-PAGE. The gel was stained briefly with Commassie blue in water and the band corresponding to GST-MIM was excised, dried and ground. The gel powder was used to raise polyclonal antisera from two rabbits through the service of Genemed Inc. The antiserum was further purified by affinity chromatography. Briefly, 0.5 mg purified His-MIM protein was conjugated to 0.2 g CNBr-activated Sepharose 4B (Amersham Biosciences) according to the manufacture's instruction. Four microliters of antiserum diluted in 20 ml PBS was loading to the affinity column, washed with PBS, eluted with 0.1M Glycine-HCl buffer, pH2.8, 0.15M NaCl. The eluate was neutralized and dialyze against PBS. The purified antibody is stored at a final concentration of 1 mg/ml.

GST, His pull down assay

To measure the affinity of MIM or MIM-CT for cortactin, 8 μg His-MIM or GST-MIM-CT were mixed with 25 μl of 50% (v/v) Ni-NTA beads or glutathione-Sepharose beads in 230 μl of 50 mM Tris-HCl (pH 8.0) containing 0.1% Triton X-100 on a rotating wheel at 4°C overnight. Beads were rinsed with the same buffer, incubated with 0.1 μM cortactin at 4°C for 2 h, washed and boiled in 12 μl 2×SDS sample buffer for 10 min. 12 μl of the sample was subjected to SDS-PAGE followed by immunoblot using anti-cortactin monoclonal antibody (4F11). The blot was digitalized by film scanning and quantified by Scion Image software.

Analysis of interaction between myc-tagged proteins and MIM

Myc-cortactin and mutant Myc-Cort-F in which tyrosine residues 421, 466 and 482 were changed to phenylalanine as previously described (10) were transfected into NIH3T3 cells expressing MIM-GFP using Superfect transfection reagent kit (Qiagen) according to the manufacture's protocol. After 24 h of transfection, cells were serum-starved overnight and treated with 30 ng/μl PDGF. At times as indicated, cell lysates were prepared and incubated at 4°C for 2 h with Myc monoclonal antibody-agarose beads (BD sciences) in lysis buffer (50 mM Tris, pH7.4, 150 mM NaCl, 1 mM EDTA, 1% Triton X-100, and 1 mM Na_3VO_4) plus protease inhibitor cocktail tablet (Roche). After two times of wash with lysis buffer, the samples were analyzed by 8% SDS-PAGE followed by immunoblot with GFP polyclonal antibody and Myc monoclonal antibody 9E10 (BD sciences), respectively.

Results

Analysis of MIM proteins in cells and tissues

To evaluate the function of MIM, we made an effort to prepare a full length murine MIM protein tagged by either 6 x His or GST epitope in bacterial strain BL21-CodonPlus-RPLI, which contains extra copies of Arg, Pro, and Leu tRNA genes, as the host for MIM. The rationale to use this host is that Arg, Pro and Leu residues are apparently over represented in the predicted MIM amino acid sequence and may quickly exhaust the limited pool of their corresponding tRNAs in common *E. Coli* strains, resulting in lower level of expression (11). With this system, we were able to prepare soluble MIM proteins in a yield over 1 mg per liter broth. The purified recombinant GST-MIM proteins were then used to raise a polyclonal antiserum, which was further purified by affinity chromatography using His-MIM conjugated Sepharose beads. The purified antibody recognizes a major cellular protein with a gel motility of 115 kDa in the whole lysate of NIH3T3 cells, which apparently comigrated with His-MIM (Fig 1A). In addition, the antibody also detected weakly a band of 150 kDa, the nature of which is currently unknown. To confirm that p115 represents MIM protein, we analyzed cell lysates from a panel of mouse tissues that are known to express MIM messengers at different levels (3). This analysis demonstrated that p115 is highly expressed in liver tissues and moderately in spleen and kidney (Fig 1B), the expression profile that is similar to that as detected by a Northern blot analysis (3). Based on a quantitative immunoblot analysis (Fig. 1A), we estimated that the cellular concentration of endogenous MIM is in a range from 3 to 5 nM in NIH3T3 cells, which is significantly lower than those of many actin cytoskeletal proteins, which normally range from several to hundreds μM (12). Therefore, it seems unlikely that MIM functions as a main structural protein in the cell. Because of its extremely low expression in most adherent cells (data

not shown), the function of MIM in cells was mainly evaluated based on epitope tagged forms that were exogenously expressed.

PDGF regulates the interaction between MIM and cortactin

Protein sequence analysis revealed that MIM is rich in proline residues in the region between amino acids 612 to 727 (Figure 3A) and contains a PPLPGPKP sequence that fits nearly an optimal sequence (PPXPXK/RP, X for an aliphatic amino acid) for binding to the cortactin SH3 domain (13;14). Therefore, we were interested in a potential interaction between MIM and cortactin. As a result, a DNA fragment encoding a full-length murine MIM protein was prepared in retroviral vector MGIN, in which MIM was tagged by GFP at its C-terminus (15). Infection of the virus into NIH3T3 cells resulted in over 90% of cell population expressing MIM-GFP based on microscopic inspection (data not shown). The level of MIM-GFP expression was about 7 folds of that of endogenous MIM as determined by immunoblot (Figure 2A). The interaction between MIM-GFP and cortactin was analyzed by immunoprecipitation of the cell lysates with GFP-antibody and followed by immunoblot with cortactin antibody. This analysis revealed that cortactin was readily coprecipitated with MIM-GFP (Figure 2B). Coprecipitation of MIM-GFP and cortactin was specific because the GFP antibody was unable to pull down cortactin in control cells infected with the vector encoding GFP only. Furthermore, cortactin antibody was also able to immunoprecipitate MIM-GFP (Figure 2B, right panel), but not GFP (data not shown).

Next, we examined whether or not the interaction between MIM-GFP and cortactin would be regulated by PDGF, which is known to induce tyrosine phosphorylation of cortactin (16). Quiescent NIH3T3 cells expressing MIM-GFP were stimulated with PDGF for times up to 30 min and the cell lysates were then subjected to immunoprecipitation with GFP antibody and followed by immunoblot with cortactin antibody. As shown in Figure 2C, a weak interaction

between MIM-GFP and cortactin was detected in the resting cells. However, the interaction was more evident upon PDGF stimulation after 1 min and decreased after 30 min, indicating that the interaction between MIM-GFP and cortactin is an early event of the PDGF signal transduction.

MIM binds to the cortactin SH3 domain through its proline rich domain

To determine whether the proline rich domain (PRD) was required for cortactin binding, we transiently transfected NIH3T3 cells with a plasmid encoding MIMΔ(612-727)-GFP protein that lacks the PRD (Figure 3A), and analyzed the ability of the mutant to bind to cortactin by immunoprecipitation analysis. As shown in Figure 3B, while MIM-GFP was readily coprecipitated with cortactin (lane 1), neither MIMΔ(612-727)-GFP nor GFP was able to coprecipitate with cortactin (lane 2 and 3). To further confirm the role of the SH3 and PRD motifs in the interaction between MIM and cortactin, we analyzed recombinant GST-MIM-CT, a short form of MIM encodes the full PRD (3) for its ability to pull down purified recombinant wild type cortactin and a cortactin mutant with the deletion of the SH3 domain. As a positive control, we also analyzed in parallel GST-Dyn-PRD, a GST-tagged peptide derived from rat dynamin 2 amino acids 747-868, which is known to bind to the cortactin SH3 domain (16). As shown in Figure 3C, although both GST-Dyn-PRD and GST-MIM-CT proteins were able to pull down effectively wild type cortactin (lane 4 and 6), they failed to precipitate the cortactin mutant lacking the SH3 domain (lane 3 and 5). GST, used as a negative control, was unable to pull down either wild type cortactin or the mutant (lane 1 and 2). Thus, the PRD of MIM is not only necessary but also sufficient to interact with cortactin in an SH3 domain dependent manner.

The interaction between MIM-GFP and cortactin within the cell was further verified by immunofluorescence analysis of NIN3T3 cells expressing MIM-GFP and MIMΔ(612-727)-GFP (Fig 4). Cortactin in cells was stained with a monoclonal antibody and GFP fusions were

visualized directly by fluorescent microscope. It is apparent that MIM-GFP colocalized with cortactin in numerous puncta of the cytoplasm (Figure 4A-C). However, the mutant MIMΔ(612-727)-GFP, which is deficient in cortactin binding, displayed a diffused staining pattern in the cytoplasm without apparent colocalization with cortactin puncta (Figure 4D-F). This result confirms that the discrete cellular distribution of MIM in cells is the result of its interaction with cortactin.

PDGF induces tyrosine phosphorylation of MIM in a Src dependent manner

Interaction with cortactin in response to PDGF implied that MIM may be involved in PDGF signal transduction. Since PDGF is known to trigger tyrosine phosphorylation of multiple cellular proteins (17), we were interested in a potential MIM phosphorylation upon PDGF treatment. As a result, quiescent NIH3T3 cells expressing MIM-GFP were treated with PDGF for various times and MIM-GFP proteins were isolated from the cell lysates by anti-GFP antibody and further immunoblotted with anti-phosphotyrosine antibody 4G10. As shown in Fig. 5A, MIM-GFP underwent a rapid tyrosine phosphorylation within 1 min, which was declined at 30 min after PDGF treatment, the kinetics that is apparently concurrent with its association with cortactin (Fig. 2C and Fig. 5C).

Src tyrosine kinase is known to be implicated in PDGF receptor signaling pathway (18) and target cortactin as well. To examine the potential role of Src in the phosphorylation of MIM, NIH3T3 cells expressing MIM-GFP were treated with PP2, a selective inhibitor of Src, for 1 h before PDGF stimulation. As shown in Fig. 5B, PP2 treatment abolished nearly completely the tyrosine phosphorylation of MIM in the course of 30 min of PDGF treatment. This data indicates that the function of Src is required for an effective tyrosine phosphorylation of MIM mediated by PDGF receptor.

Tyrosine phosphorylation of cortactin is required for its effective association with MIM

Next, we examined whether tyrosine phosphorylation regulates the interaction between MIM and cortactin. The PP2 treated quiescent cells were stimulated with PDGF, lysed and immunoprecipated with GFP antibody followed by immunoblot with cortactin antibody. As shown in Fig. 5C, interaction between cortactin and MIM-GFP, as shown by cortactin bands, at 1 and 5 min in the PP2 treated cells after PDGF treatment was nearly abolished, although a slight increase in the reaction started to be visible at 10 and 30 min. Therefore, the kinase activity of Src is required for an efficient interaction between cortactin and MIM at least during an early phase of PDGF signal transduction.

PDGF also induces tyrosine phosphorylation of cortactin as early as 1 min and decreased after 10 min (Fig. 6A), the kinetics that was similar to that of phosphorylation of MIM-GFP (Fig. 5A) and that of the interaction between MIM-GFP and cortactin (Fig. 2C). To examine the role of tyrosine phosphorylation of cortactin in its interaction with MIM, Myc-cortactin and a mutant Myc-Cort-F in which Src targeted tyrosine residues 422, 461 and 482 have been changed to phenylalanine (9), were transiently transfected into NIH3T3 cells expressing MIM-GFP. The transfected cells were starved overnight, treated with PDGF and subjected to immunoprecipitation with GFP antibody. The precipitates were then immunoblotted with monoclonal antibody 9E10 against Myc epitope. As shown in Fig. 6B, top panel, the kinetic interaction of MIM-GFP with Myc-cortactin was quite similar to that with endogenous cortactin as it increased at 5 and 10 min after PDGF treatment. However, under the same condition, PDGF failed to induce any apparent increase in the interaction between Myc-Cort-F and MIM-GFP (Fig. 6B, lower panel). This data indicates that the PDGF mediated interaction between MIM and cortactin requires tyrosine phosphorylation of cortactin.

13

Discussion

MIM is an interesting molecule because it may act potentially as a metastasis suppressor. While the presence of abundant MIM messengers in tissues and a few cell lines has been reported (3), expression of MIM proteins in cells had not yet been confirmed. The presented study demonstrated for the first time that MIM protein is expressed in cells and certain tissues. With a polyclonal antibody against full-length MIM, we were able to detect a dominant band with a gel motility of 115 kD, which comigrates with recombinant full-length MIM proteins. This apparent molecular size as determined by SDS-PAGE is significantly larger than 82 kD, as predicted from the amino acid sequence. The authenticity of the p115 as MIM was further verified by an observation that the antibody recognizes specifically MIM-GFP in both immunoblotting and immunostaining analyses (data not shown). Furthermore, the profile of p115 expression in several tissues is consistent with that of MIM messengers as determined by Northern blot because both p115 and MIM mRNA appear to be the most abundant in the liver (3). However, the level of MIM protein expression in many cell lines appeared to be low. Based on immunoblot, we estimated that the cellular concentration of MIM in NIH3T3 cells is approximately from 3 to 5 nM, which is significantly lower than cortactin (2 μM) and many other actin binding proteins (12). The low level of MIM protein in most cells supports the view that MIM acts as a signaling molecule, rather than as a structural protein, and may bind to cortactin only in certain cellular locations where growth factor signaling molecules are also present. Such timely and spatial interaction between MIM and cortactin within cells may represent a novel mechanism for extracellular stimuli to regulate the actin dynamics.

Consistent with its signaling function, the data presented here also demonstrated for the first time that MIM is implicated in PDGF signal transduction. Tyrosine phosphorylation of

MIM-GFP is a rapid event and occurs as early as 1 min after PDGF stimulation. The kinetics of tyrosine phosphorylation of MIM is correlated with its association with cortactin as well as phosphorylation of cortactin. Inhibition of the Src activity by PP2 abolished both MIM-GFP phosphorylation as well as the interaction with cortactin. Furthermore, PDGF failed to induce increase in the association of MIM-GFP with a cortactin mutant deficient in tyrosine phosphorylation, indicating that tyrosine phosphorylation of cortactin plays an essential role in the PDGF mediated increase in its association with MIM. Cortactin is known to bind to multiple cellular proteins through its SH3 domain, including dynamin 2, ZO-1, N-WASP, CBP90, CortBP-1, CD2AP, WIP, MLCK, Fdg1 and BPGAP1 (16;19-27). However, the potential regulation of the interaction with most of these proteins in cells by growth factors has not yet been extensively investigated. A recent study reported that EGF induces recruitment of cortactin to CD2AP, which is also a cortactin SH3 binding protein, in MDA-MB-231 cells (23). While it is unclear whether such interaction requires tyrosine phosphorylation, it has been reported that EGF triggers tyrosine phosphorylation of cortactin as well (28), supporting the possibility that tyrosine phosphorylation regulates the interaction of cortactin with CD2AP. This phosphorylation dependence may be due to increase in the access of cellular proteins to the SH3 domain of phosphorylated cortactin through a possible releasing from an antoinhibition of configuration (29), although the detail of this possible antoinhibition has not yet been defined. It is also possible that tyrosine phosphorylation may be required for cortactin to translocate into a special cellular compartment where it forms a complex with MIM. In fact, our recent study has shown that tyrosine phosphorylation triggers the translocation of a cortactin like protein HS1 into lipid rafts of lymphocytes (30), a membrane microdomain where many phosphorylated proteins, kinases and cytoskeletal proteins are frequently accumulated. It is of interest to note that MIM

associates with membrane bound protein tyrosine phosphatase δ (2). Certain membrane protein tyrosine phosphatases such as CD45 are known to exclude from lipid rafts (31). Therefore, it is possible that PDGF may provoke a change in the interaction between MIM and protein phosphatases, resulting in a transient distribution of MIM into lipid rafts where it meets with phosphorylated cortactin. Further study is needed to distinguish these possibilities.

Reference List

1. Lee, Y. G., Macoska, J. A., Korenchuk, S., and Pienta, K. J. (2002) *Neoplasia.* **4,** 291-294

2. Woodings, J. A., Sharp, S. J., and Machesky, L. M. (2003) *Biochem. J.* **371,** 463-471

3. Mattila, P. K., Salminen, M., Yamashiro, T., and Lappalainen, P. (2003) *J. Biol. Chem.* **278,** 8452-8459

4. Yamagishi, A., Masuda, M., Ohki, T., Onishi, H., and Mochizuki, N. (2004) *J. Biol. Chem.*

5. Bubb, M. R., Lewis, M. S., and Korn, E. D. (1991) *J. Biol. Chem.* **266,** 3820-3826

6. Safer, D., Elzinga, M., and Nachmias, V. T. (1991) *J. Biol. Chem.* **266,** 4029-4032

7. Uruno, T., Liu, J., Zhang, P., Fan, Y., Egile, C., Li, R., Mueller, S. C., and Zhan, X. (2001) *Nat. Cell Biol.* **3,** 259-266

8. Zhan, X., Hu, X., Hampton, B., Burgess, W. H., Friesel, R., and Maciag, T. (1993) *J. Biol. Chem.* **268,** 24427-24431

9. Huang, C., Ni, Y., Wang, T., Gao, Y., Haudenschild, C. C., and Zhan, X. (1997) *J. Biol. Chem.* **272,** 13911-13915

10. Huang, C., Liu, J., Haudenschild, C. C., and Zhan, X. (1998) *J. Biol. Chem.* **273,** 25770-25776

11. Makrides, S. C. (1996) *Microbiol. Rev.* **60,** 512-538

12. Pollard, T. D., Blanchoin, L., and Mullins, R. D. (2000) *Annu. Rev. Biophys. Biomol. Struct.* **29,** 545-576

13. Sparks, A. B., Rider, J. E., Hoffman, N. G., Fowlkes, D. M., Quillam, L. A., and Kay, B. K. (1996) *Proc. Natl. Acad. Sci. U. S. A* **93,** 1540-1544

14. Yamabhai, M. and Kay, B. K. (1997) *Anal. Biochem.* **247,** 143-151

15. Cheng, L., Du, C., Murray, D., Tong, X., Zhang, Y. A., Chen, B. P., and Hawley, R. G. (1997) *Gene Ther.* **4,** 1013-1022

16. McNiven, M. A., Kim, L., Krueger, E. W., Orth, J. D., Cao, H., and Wong, T. W. (2000) *J. Cell Biol.* **151,** 187-198

17. Claesson-Welsh, L. (1994) *Prog. Growth Factor Res.* **5,** 37-54

18. Courtneidge, S. A., Fumagalli, S., Koegl, M., Superti-Furga, G., and Twamley-Stein, G. M. (1993) *Dev. Suppl* 57-64

19. Katsube, T., Takahisa, M., Ueda, R., Hashimoto, N., Kobayashi, M., and Togashi, S. (1998) *J. Biol. Chem.* **273,** 29672-29677

20. Kinley, A. W., Weed, S. A., Weaver, A. M., Karginov, A. V., Bissonette, E., Cooper, J. A., and Parsons, J. T. (2003) *Curr. Biol.* **13,** 384-393

21. Ohoka, Y. and Takai, Y. (1998) *Genes Cells* **3,** 603-612

22. Du, Y., Weed, S. A., Xiong, W. C., Marshall, T. D., and Parsons, J. T. (1998) *Mol. Cell Biol.* **18,** 5838-5851

23. Lynch, D. K., Winata, S. C., Lyons, R. J., Hughes, W. E., Lehrbach, G. M., Wasinger, V., Corthals, G., Cordwell, S., and Daly, R. J. (2003) *J. Biol. Chem.* **278,** 21805-21813

24. Dudek, S. M., Jacobson, J. R., Chiang, E. T., Birukov, K. G., Wang, P., Zhan, X., and Garcia, J. G. (2004) *J. Biol. Chem.*

25. Kim, K., Hou, P., Gorski, J. L., and Cooper, J. A. (2004) *Biochemistry* **43,** 2422-2427

26. Lua, B. L. and Low, B. C. (2004) *Mol. Biol. Cell*

27. Weaver, A. M., Heuser, J. E., Karginov, A. V., Lee, W. L., Parsons, J. T., and Cooper, J. A. (2002) *Curr. Biol.* **12,** 1270-1278

28. Maa, M. C., Wilson, L. K., Moyers, J. S., Vines, R. R., Parsons, J. T., and Parsons, S. J. (1992) *Oncogene* **7,** 2429-2438

29. Martinez-Quiles, N., Ho, H. Y., Kirschner, M. W., Ramesh, N., and Geha, R. S. (2004) *Mol. Cell Biol.* **24,** 5269-5280

30. Hao, J. J., Carey, G. B., and Zhan, X. (2004) Syk-mediated tyrosine phosphorylation is required for the association of HS1 with lipid rafts and BCR signalosome complex.

31. Cheng, P. C., Dykstra, M. L., Mitchell, R. N., and Pierce, S. K. (1999) *J. Exp. Med.* **190,** 1549-1560

Figure Legends

Figure 1. Analysis of MIM protein expression in cells and tissues. (A) Total cell lysates from different numbers of NIH3T3 cells as indicated were separated by SDS-PAGE, transferred to a membrane and immunoblotted with affinity purified anti-MIM antibody. As controls, purified recombinant His-MIM at different amounts were also analyzed in the same gel. The positions for p150 (minor band) and p115 (major band) were indicated by arrows. The band of p115 was apparently aligned with that of recombinant His-MIM. **(B)** Tissues from an adult mouse were isolated and lysed by homogenization. Aliquots of tissues lysates were separated by SDS-PAGE and further immunoblotted with anti-MIM antibody. Lane 1, 0.5 ng His-MIM; lane 2, heart; lane 3, kidney; lane 4, liver; lane 5, spleen; and lane 6, molecular weight markers.

Figure 2. MIM is a cortactin binding protein. (A) Immunoblot analysis of MIM-GFP expression in NIH3T3 cells. NIH3T3 cells infected with retroviruses carrying either GFP or MIM-GFP were lysed. The lysates were analyzed by immunoblot using MIM antibody. The positions representing MIM-GFP and endogenous MIM were indicated by arrows. Multiple lower bands shown in the 3T3/MIM-GFP lane likely represent degraded MIM-GFP. **(B)** Analysis of the interaction between cortactin with MIM. Left panel. NIH3T3 cells expressing MIM-GFP or GFP only were immunoprecipitated with polyclonal GFP antibody. The pellets were separated by SDS-PAGE and then immunoblotted with cortactin monoclonal antibody (4F11). The same blot was stripped and reblotted with GFP antibody to confirm the expression of MIM-GFP (lower panel). Right panel. The above cell lysates were immunoprecipitated first with polyclonal cortactin antibody and the pellets were fractionated by SDS-PAGE, transferred to a membrane and analyzed for the presence of MIM-GFP by immunoblot analysis using GFP-antibody. The same membrane was also blotted with cortactin antibody. **(C)** PDGF induces the

interaction between cortactin and MIM. Starving NIH3T3 cells expressing MIM-GFP were treated with PDGF for 0 to 30 min. The cell lysates were immunoprecipitated with GFP antibody. The pellets were then blotted with cortactin antibody (4F11) and reblotted with monoclonal GFP antibody.

Figure 3. MIM binds to the SH3 domain of cortactin. (**A**) Schematic presentation of MIM and its variants. IMD: IRsp53 and MIM homology domain; CC: coiled-coil domain; LRD: Lysine rich domain; SRD: serine rich domain; PRD: proline rich domain; and WH2: WASP homology 2 domain. (**B**) MIM requires its PRD to bind to cortactin. NIH3T3 cells expressing MIM-GFP or MIMΔ(612-727)-GFP were lysed and immunoprecipitated with polyclonal GFP antibody. The pellets were then immunoblotted with cortactin antibody (top panels) and then reblotted with monoclonal GFP antibody (lower panels). The position of cortactin was indicated by an arrow. (**C**) Cortactin SH3 domain is required to bind to MIM. Purified GST, GST-Dyn-PRD and GST-MIM proteins (8 μg) were incubated with either 100 nM His-cortactin (lanes 2, 4 and 6) or 100 nM His-CortΔSH3 (lanes 1, 3 and 5), and 25 μl of glutathione beads at 4°C. The pellets were separated by SDS-PAGE followed by immunoblot with cortactin antibody.

Figure 4. MIM-GFP colocalizes with cortactin. NIH3T3 cells expressing MIM-GFP (**A-C**) or NIH3T3 cells expressing MIMΔ(612-727)-GFP (**D-F**) grown on fibronectin coated glass cover slips were stained with polyclonal GFP antibody (green) and monoclonal cortactin antibody (red). The cells were inspected under a fluorescent microscope using a 60 x oil lens. The cell digital images were captured and further processed by Adobe Photoshop.

Figure 5. PDGF induces tyrosine phosphorylation of MIM and interaction between MIM and cortactin. (A) Quiescent NIH3T3 cells expressing MIM-GFP were stimulated with 30 ng/ml PDGF for different times as indicated. After stimulation, cells were lysed,

immunoprecipitated with GFP antibody and further blotted with monoclonal phosphotyrosine antibody (4G10). The same blot was stripped and reprobed with GFP antibody to show the loading control. (**B**) Starving NIH3T3 cells expressing MIM-GFP were treated with or without PP2 for 20 min prior to PDGF treatment. The treated cell lysates were immunoprecipitated with GFP antibody. The pellets were immuunoblotted with cortactin antibody (top panels) and reblottd with monoclonal GFP antibody (bottom panels). (**C**) NIH3T3 cells expressing MIM-GFP were treated as in B. The cell lysates were immunoprecipitated with GFP antibody and were blotted with cortactin antibody (upper panels) and reblotted with GFP antibody.

Figure 6. Tyrosine phosphorylation of cortactin is required for PDGF induced interaction between MIM and cortactin. (**A**) Quiescent NIH3T3 cells were stimulated with PDGF for the times as indicated. The lysates of the stimulated cells were immunoprecipitated with anti-cortactin antibody and further analyzed by immunoblotting with phosphotyrosine antibody 4G10. The same membrane was also re-probed with anti-cortactin antibody. (**B**) NIH3T3 cells expressing MIM-GFP were transiently transfected with either Myc-Cort (upper panel) or Myc-Cort-F (lower panel). The transfected cells were rested in a serum-free medium and stimulated with PDGF. The cell lysates were immunoprecipiated with Myc antibody (9E10) and the pellets were immunoblotted with GFP. The same blots were also stripped and probed with Myc antibody to show the loading control.

Acknowledgments